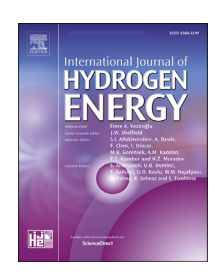


Available online at www.sciencedirect.com

ScienceDirect





Renewable hydrogen from glycerol steam reforming using Co-Ni-MgO based SBA-15 nanocatalysts



S. Al-Salihi ^b, R. Abrokwah ^{a,d}, W. Dade ^a, V. Deshmane ^{a,b}, T. Hossain ^{a,b}, D. Kuila ^{a,c,d,*}

- ^a Department of Chemistry, North Carolina A & T State University, Greensboro, NC 27411, USA
- ^b Department of Chemical Engineering, North Carolina A & T State University, Greensboro, NC 27411, USA
- ^c Department of Nanoengineering, Joint School of Nanoscience and Nanoengineering, North Carolina A & T State University, Greensboro, NC 27411, USA
- ^d Energy and Environmental Systems, North Carolina A & T State University, Greensboro, NC 27411, USA

HIGHLIGHTS

- M-SBA-15, M-MgO-SBA-15 (M = Co, Ni) and Co-Ni-SBA-15 were prepared by one-pot method.
- XRD confirmed the presence of active NiCo₂O₄ spinel crystal phase in the catalysts.
- Bimetallic catalysts were more active toward glycerol reforming at as low as 450 °C.
- Cobalt exhibited better GSR activity and higher stability than nickel catalysts.
- MgO addition to Ni-SBA-15 decreased carbon deposition on the catalyst by 66%.

ARTICLE INFO

Article history:
Received 23 September 2019
Received in revised form
1 March 2020
Accepted 18 March 2020
Available online 22 April 2020

Keywords:

One-pot hydrothermal synthesis Impregnation Glycerol steam reforming Mesoporous silica Co-Ni bimetallic Catalysts MgO modified-SBA-15 catalysts

ABSTRACT

Steam reforming of glycerol was carried out using Si-based mesoporous SBA-15 catalysts. Different mesoporous catalysts- Co-SBA-15, Ni-SBA-15, Co-MgO-SBA-15, Ni-MgO-SBA-15, and Co-Ni-SBA-15 were prepared using a one-pot hydrothermal method. An incipient wetness impregnation method was used only for the bimetallic Co-Ni-SBA-15 catalyst (catalyst designated as Co-Ni-SBA-15-IMPG) to compare its activity to that prepared by the one-pot method. The catalysts were characterized using XRD, TPR, TEM, TGA-DSC, ICP-OES and N_2 adsorption-desorption analytical techniques. A high surface area in the range of 540 -750 m²/g was observed depending on the catalyst composition. The glycerol steam reforming (GSR) activity of the catalysts was studied in the reaction temperature range of $450~^{\circ}\text{C}-700~^{\circ}\text{C}$ for hydrogen production. Results from the GSR studies for continuous 40~hshowed that both Co-Ni-SBA-15-IMPG (impregnation) and Co-Ni-SBA-15 (one-pot) were resistant to deactivation, and both yielded 100% glycerol conversion for the entire 40 h. 10% Co-5%Ni-SBA-15 and 10%Co-5%Ni-SBA-15-IMPG produced (70-78) % and (60-78) % ${\rm H}_2$ selectivity, respectively. Addition of MgO to Co-SBA-15 and Ni-SBA-15 increased the activity and stability of the catalysts. The catalyst stability performance followed the trend 10%Co-5%Ni > 10%Co-5%MgO >10%Co-5%Ni-IMPG. > 15%Co > 10%Ni-5%MgO >15%Ni-SBA-15. Thermal analyses of the spent catalyst showed a substantial amount of coke deposition which could be the major factor responsible for catalysts deactivation. Bimetallic catalysts prepared by one-pot method (10%Co-5%Ni-SBA-15) and incipient wetness

^{*} Corresponding author. Department of Chemistry, North Carolina A & T State University, Greensboro, NC 27411, USA. E-mail address: dkuila@ncat.edu (D. Kuila).

impregnation (10%Co-5%Ni-SBA-15-IMPG) exhibited remarkable GSR activity compared to their monometallic counterparts. The GSR activity was observed in the order: 10%Co-5% Ni-IMPG \geq 10%Co-5%Ni > 10%Co-5%MgO >15%Co > 15%Ni > 10%Ni-5%MgO.

© 2020 Hydrogen Energy Publications LLC. Published by Elsevier Ltd. All rights reserved.

Introduction

The continuous need to develop and improve alternative sources of energy has led researchers to recent advances in fuel cell technology. Hydrogen powered fuel cell devices efficiently convert chemical energy into electrical power with little to no emission of pollutants [1-4] and can overcome the challenges of hydrogen storage and transportation. Hydrogen can be produced by steam reforming of methanol [5,6], ethanol and glycerol [7], liquefied natural gas (LNG) [5]; windbased water electrolysis [8,10], solar thermal water splitting [9,11], biological water splitting [10], fermentation and biomass gasification [11]. In United States, H2 is mostly produced by steam reforming of natural gas and scientists are developing advanced processes to produce H2 with zero detrimental environmental impact and maximum energy efficiency. Renewable biomass is an attractive source relative to fossil feedstocks such as natural gas and coal because it has negligible impact on CO₂ pollution. Further, the hydrogen task force team, from the Paris Agreement Convention in 2016, charged government institutions and declared that reduction of global warming to no more than a 2 °C increase will require an exceptional and enduring effort, such as complete decarbonization of a large section of the energy systems through accelerated hydrogen technology designs, applications and consumption [12].

Recently, steam reforming of bio-derived liquids to produce H2 has attracted great interest due to environmental concerns and increasing demand of H₂ in various applications, especially for the proton exchange membrane fuel cells (PEMFC). Glycerol, readily available as a by-product in biodiesel industry, has received wide attention as it contains higher moles of H₂ than methanol or ethanol [13]. It has been reported that by 2020, three megatons of crude glycerol is expected to be produced [14]. The demand for H2 from glycerol will also benefit the economics of the biodiesel industry. Glycerol reforming in the presence of a catalyst is overall an endothermic reaction because heat required for glycerol decomposition is much higher than heat produced in the water gas shift reaction. In the overall reforming reaction, 7 mols of H₂ are produced per mol of glycerol consumed: $C_3H_8O_3 + 3H_2O \Leftrightarrow 7H_2 + 3CO_2$. Excess steam and high temperature shifts the reaction equilibrium forward and therefore more H₂ is produced. The reforming reaction is a combination of glycerol decomposition ($C_3H_8O_3 \Leftrightarrow 4H_2 + 3CO$) and watergas shift reaction (CO + $H_2O \Leftrightarrow H_2 + CO_2$). Methanation reactions also occur whereby CH4, an undesirable product, is formed by reaction of H2 with either CO or CO2, thus minimizing H₂ selectivity. Also, the steam reforming and the water gas shift reactions are reversible which can lead to CO and ${\rm CH_4}$ formation depending on the reaction conditions.

Suitable catalysts such as group 8, 9 and 10 metals are usually utilized for the activation and oxidation of CH4 to syngas ($CO + H_2$). The CO is then consumed by the water gas shift (WGS) reaction to produce an extra mole of H2 and CO2 [15]. Deactivation of the catalysts by carbon deposition and thermal sintering under GSR operating conditions are major challenges of GSR reactions. However, specific metalsupport interactions have been reported to help alleviate quick catalyst deactivation and improve their activity during steam-reforming reactions [18,19]. Various catalysts such as Ni, Co, Pt, Ru, and Rh have been investigated for the GSR reactions [16]. Zhang et al. [17] reported that Ir/CeO₂ catalyst exhibited more than 85% hydrogen selectivity and 100% glycerol conversion at 400 °C using volume ratios of $C_3H_8O_3/H_2O/He = 2/18/80$. Their TPR profiles showed that the stronger metal-support interaction in Ir/CeO2 catalyst compared to Co/CeO2 and Ni/CeO2 contributed to the better performance of Ir/CeO2 catalyst. Hirai et al. [18] conducted glycerol steam reforming in the temperature range of 500–600 $^{\circ}$ C and found ruthenium supported on Y_2O_3 (3 wt% Ru/Y₂O₃) exhibited higher hydrogen yield and glycerol conversion compared to Ruthenium supported on MgO and Al₂O₃. A fluidized bed reactor used by Czernik et al. [19] for hydrogen production from different biomass-derived liquids including crude glycerol yielded 74% hydrogen at 850 °C using Ni/Al₂O₃ catalyst and 2:1 steam to glycerol molar ratio. Adhikari et al. [20] found that Ni/Al₂O₃ and Rh/CeO₂/Al₂O₃ were the best performing catalysts in terms of hydrogen selectivity and glycerol conversion and concluded that with the increase in water to glycerol molar ratio, both hydrogen selectivity and conversion of glycerol increased.

There are several reports on the ease of deactivation of Ni catalysts by carbonaceous by-products compared to Cobased catalysts. Alaric C.W. Koh and coworkers [21] worked with supported nickel-cobalt catalysts. They observed that during the partial oxidation of methane, the stability and coke resistance ability of the nickel catalysts increased as the loading/ratio of cobalt in the bimetallic catalysts increased. They concluded that whiles cobalt was very efficient with the conversion of carbon/soot to CO and CO₂, the nickel catalyst showed superior short-term activity but was vulnerable to coke poisoning and deactivated quickly. Sanchez and Comelli [22] also studied the alumina supported cobalt and nickel catalysts for hydrothermal production of hydrogen from glycerol. They noticed that for the bimetallic 4Co4Ni/Al₂O₃ at 300 °C, the amount of hydrogen increased from about 65% to 84% when the cobalt fraction was increased from 4 wt% to 12 wt%. They inferred

that compared to Ni, Co catalysts were active at low temperature and exhibited better stability during the reaction. Busca et al. [23] also reported that during ethanol steam reforming, Co–Zn–Al mixed oxide catalysts performed better than Ni–Zn–Al ones prepared by the same hydrotalcite precursors. They concluded that in the 720 K–870 K temperature range the addition of cobalt increased the selectivity of hydrogen and $\rm CO_2$ but decreased the selectivity of CH₄. Other researchers have independently corroborated the high stability of cobalt catalysts relative to that of nickel [24–26].

Ordered mesoporous silica and titania supports have also been used for GSR because they exhibit high thermal and chemical stability as well as defined tunable pore size and high surface area for catalytic applications [27,28]. More specifically, the SBA-15 support has been confirmed to promote activity, selectivity, and stability of the catalyst in GSR studies [29]. In this study, the effects of Ni-, Co- and Ni-Co bimetallic catalysts immobilized on SBA-15 support was investigated for steam reforming of glycerol to understand the effect of bimetallic catalysts and metal-support interactions on H2 production. Additionally, to enhance catalyst stability and decrease rate of deactivation, we also investigated the extent to which the addition of alkaline MgO to SBA-15 support could help neutralize the acidic coke deposits on the active sites. Our goal is to explore hydrogen production using these modified mesoporous SBA-15 frameworks to understand their interaction with nanocatalysts to help identify the most efficient and effective catalyst system for GSR and related studies.

Experimental

Materials and methods

Tetraethyl orthosilicate, 98% (TEOS), cetyltrimethyl ammonium bromide, 99% (CTAB), magnesium nitrate hexahydrate (99%), cobalt chloride hexahydrate, and Pluronic acid (P-123) were obtained from Sigma Aldrich, Missouri, USA. Nickel nitrate hexahydrate, ethanol, hydrofluoric acid (51%), nitric acid (68%), glycerol (99.6%), and potassium bromide were purchased from Fisher Scientific, New Jersey, USA. The distilled water used in the experimental work was purified utilizing Mill-Q Advantage A10 Elix 5 system acquired from Millipore Corporation (Bedford, MA, USA).

Experimental procedure

The catalysts were prepared using: (1) a one-pot process and (2) Incipient wetness impregnation method. In the one-pot process, TEOS, CTAB, water, ethanol, pluronic, and hydrochloric acid were mixed in molar ratio of 1 TEOS: 0.081 CTAB: 41 $\rm H_2O$: 7.5 ethanol: 0.01679 Pl23: 5.981 HCl. In a typical process, P123 was dissolved in 2 M HCl at 35 °C to get a clear solution designated as solution "A". Another solution designated as "B" was prepared by dissolving CTAB in DI water and stirring at 35 °C until a colorless, homogenous mixture was

obtained. Solution B was then gently poured into solution A with continuous stirring for 30 min and resulted in solution C. Ethanol containing the metal precursors was added dropwise to solution C and stirred for 30 min. Afterwards, TEOS was added dropwise into solution C and stirred for 20 h at 35 °C for aging. The final aqueous mixture was then aged at 98 °C in the oven for 48 h followed by air-drying for under fume hood for 24 h. The mixture (now a white precipitate) was then ovendried again for 24 h at 98 °C. Finally, the dried material was calcined in a stepwise fashion at 1 °C/min at 350 °C for 8 h, 1 °C/min at 450 °C for 8 h, and 1 °C/min at 550 °C for 8 h. For the incipient wetness impregnation method to prepare 10% Co-5%Ni-SBA-15-IMPG, the required quantity of Ni (NO₃)₂·6H₂O and CoCl₂·6H₂O were dissolved in ethanol to form a solution. This solution was then added to 5.1 g of calcined SBA-15 and was thoroughly mixed to obtain a homogenous mixture. The slurry of impregnated catalyst was air-dried overnight and calcined at 550 °C for 6 h at a heating rate of 1 °C/min.

The catalytic activity tests were conducted within a temperature range of 450 and 700 °C. Glycerol steam reforming was carried out using a set-up built in our laboratory. The calcined catalysts were first reduced ex-situ in a furnace under 10% H₂-Ar mixture environment at 550 °C for 6 h. The reduced catalyst (around 0.7-1.3 g) was mixed with 50-70 mesh quartz sand (supplied by Sigma-Aldrich) at an equal volume ratio to minimize hot spot effects. The mixture was loaded into a stainless-steel fixed bed up-flow reactor (Tube ID: 10.2 mm) with quartz wool placed at each end to seal and prevent catalyst migration from the reactor. Prior to the reaction, the catalyst was reduced again (in-line) under 10% H₂ and Ar environment at 550 °C for 1 h. Afterwards catalysts testing was carried out at atmospheric pressure. In this process, a liquid feed mixture of glycerol/water (molar ratio of 1:12) was introduced at a constant flow rate (by HPLC pump) of 0.2 ml/min through an evaporation chamber into the reactor and then a condenser (cold trap). The noncondensable gaseous products were analyzed using an inline Agilent 7890B GC equipped with thermal conductivity detector (TCD). Nitrogen gas was used to bolster the flow of the gaseous feed through an Alborg mass flow controller at 50 ml/min at STP as well as an internal standard for subsequent chromatographic quantification. Selectivity was determined by analyzing the moles of H2, CO, CH4 and CO2 produced in the GSR reaction. Glycerol conversion, selectivity towards the gaseous reformates were calculated using equations (1)–(3). At the end of each steam reforming run, the catalyst was regenerated at 450 °C and reused. The regeneration was done under a continuous flow of air while monitoring the CO2 peak in GC until it disappeared. A complete deactivation study was conducted for all catalysts on stream for 40 h at 650 °C as it was the optimum temperature to yield the best H₂ selectivity.

%
$$H_2$$
 Selectivity = $\frac{H_2 \text{ moles produced}}{C \text{ atoms in the feedstock}} \times \frac{1}{RR} \times 100$ (1)

where, RR is the reforming ratio (7/3), defined as the ratio of moles of H_2 to CO_2 formed.

% Selectivity of CO =
$$\frac{\text{CO moles in product}}{\text{CO moles in product} + \text{CO}_2 \text{ moles in product} + \text{CH}_4 \text{ moles in product}} \times 100$$
 (2)

% Glycerol Conversion =
$$\frac{(CO_2 + CO + CH_4) \ \textit{mole produced}}{3 \times (\textit{mol glycerol in the feed})} \times 100 \tag{3}$$

Catalyst characterization and results

The Thermo-gravimetric analyzer (TGA) coupled with differential scanning calorimetry (DSC) (SDT Q600 V20.3 Build 14 system TA Instruments), was used to monitor the thermal behavior of the as-prepared and spent catalysts. The airflow rate in the chamber was kept constant at 100 ml/min and the sample was heated at the rate of 10 °C/min. Specific surface area, pore size, pore volume and pore size distribution (PSD) were measured by nitrogen adsorption-desorption at 77 K using a Quantachrome NOVA 2200e instrument. Nitrogen is the most widely used adsorbate [30]. However, we must point out that for heterogeneous surfaces with pores smaller than 2 nm, argon which is a monoatomic molecule, more spherical and relatively less reactive provides more accurate results [31]. Prior to adsorption analysis, most of the samples were outgassed under vacuum at 150 °C for 5 h. Surface areas were determined by employing the Brunauer-Emmett-Teller (BET) model, and the total pore volume was found as a function of the amount of nitrogen adsorbed at a relative pressure of unity using the density functional theory (DFT).

The Inductively coupled plasma optical emission spectroscopy, ICP-OES Agilent 710-ES spectrometer was used to determine the actual metal content in the catalysts. First, solid samples of the catalyst were dissolved by acidic digestion inside a Teflon beaker, in which a 75 mg sample was dissolved in a mixture that consists of 2 ml concentrated hydrofluoric acid (51% HF) and 3 ml concentrated nitric acid (68% HNO₃). Then, the sample was heated at about 80 °C for 10 min and diluted to the desired parts per million with de-ionized water before ICP-OES analysis.

D8 Discover X-ray diffractometer (Bruker Optics, Inc., Billerica, MA) was utilized to record the low and wide angle XRD patterns with a point detector from 1° to 8° and 20° to 80° scattering angle (20) respectively. Cu K α radiation generated at 40 mA and 40 kV at the scanning rate of 0.01°/s was used. The crystal sizes of the monoclinic and tetragonal phases were determined using the Scherrer equation expressed as: $\tau=0.9\lambda/\beta cos\theta$, where $\tau=crystal$ size; $\lambda=$ wavelength of the Cu K α radiation; $\beta=$ full-width half maximum of the respective peak; and $\theta=$ Braggs angle of diffraction.

Hydrogen temperature programmed reduction (H_2 -TPR) measurements were performed on the AutoChem II 2920 Chemical Analyzer from Micro Instrument Corp., USA. 0.05 g of catalyst was loaded into a fixed-bed clean quartz sample cell. In this process, the continuous temperature change was monitored by a thermocouple embedded in the quartz sample

cell. Prior to H₂-TPR measurements, the sample was flushed with 10% H₂ in pure argon flow of 50 ml/min with a heating rate of 10 °C/min. The sample analysis was started under H₂–Ar flow (50 ml/min) at 200 °C for 30 min, then ramped at 10 °C/min to the final temperature of 1000 °C and finally allowed to cool to room temperature at a ramp rate of 50 ml/min.

The morphology and porosity of the catalysts was analyzed using transmission electron microscopy (TEM). Micrographs of samples were acquired on Zeiss Libra 120 transmission electron microscope equipped with an accelerating voltage of 120 kV. The catalyst samples were dissolved in ethanol, deposited by a pipet on carbon-coated microgrid and oven dried at $100\,^{\circ}\text{C}$ for 12 h before imaging. The elemental compositions and distribution within the mesoporous support was observed by an energy dispersive X-ray spectroscopy (EDX)-Zeiss EVO LS10 scanning electron microscopy (SEM) equipped with Oxford INCA X-act detector.

Thermal and calorimetric analysis of M-SBA-15 samples

Fig. 1a shows the TGA-DSC profile of as-prepared (not calcined) mesoporous SBA-15 support. The thermogram comprises of three weight loss stages. The first one below 180 °C is ascribed to the removal of water/moisture adsorbed on SBA-15 surfaces. The second weight loss between 180 °C and 250 °C that centers at 200 °C is attributed to decomposition of the pluronic acid (P123) template used for synthesis. The last peak centered around 290 °C in between 250 °C and 390 °C occurred as a result of the removal/decomposition of the surfactant CTAB. No weight loss was observed between 400 °C and 1000 °C suggesting that SBA-15 support is thermally stable up to; and even beyond 1000 °C. The thermal profiles of metal-incorporated catalysts systems exhibited similar weight loss patterns as described above and additional thermograms at higher temperature. As an archetype, the thermal decomposition profiles of 15%Co-SBA-15 and 10%Co-5%MgO-SBA-15 are shown in Fig. 1b. In the case of 15%Co-SBA-15, the exothermic weight loss centered around 330 °C is associated with decomposition of the cobalt precursor- COCl₂·6H₂O, while the miniature weight loss at 550 °C has been reported to be caused by decomposition of the precipitated cobalt hydroxide to the oxide [32]. Similarly, the weight change for 10% Co-5%MgO-SBA-15 at ~328 °C is due to volatilization of the cobalt precursor and the peak around 450 °C represents decomposition of Mg(NO₃)₂ to MgO [33].

X-ray diffraction of different M-SBA-15 and ICPOES analysis of catalysts

Powder X-ray diffraction technique wasused to determine the crystal lattice parameters of the mesoporous catalysts. Fig. 2(a) and (b), shows the small angle XRD (SXRD) of the host catalyst support SBA-15 and Co/Ni incorporated catalysts. The

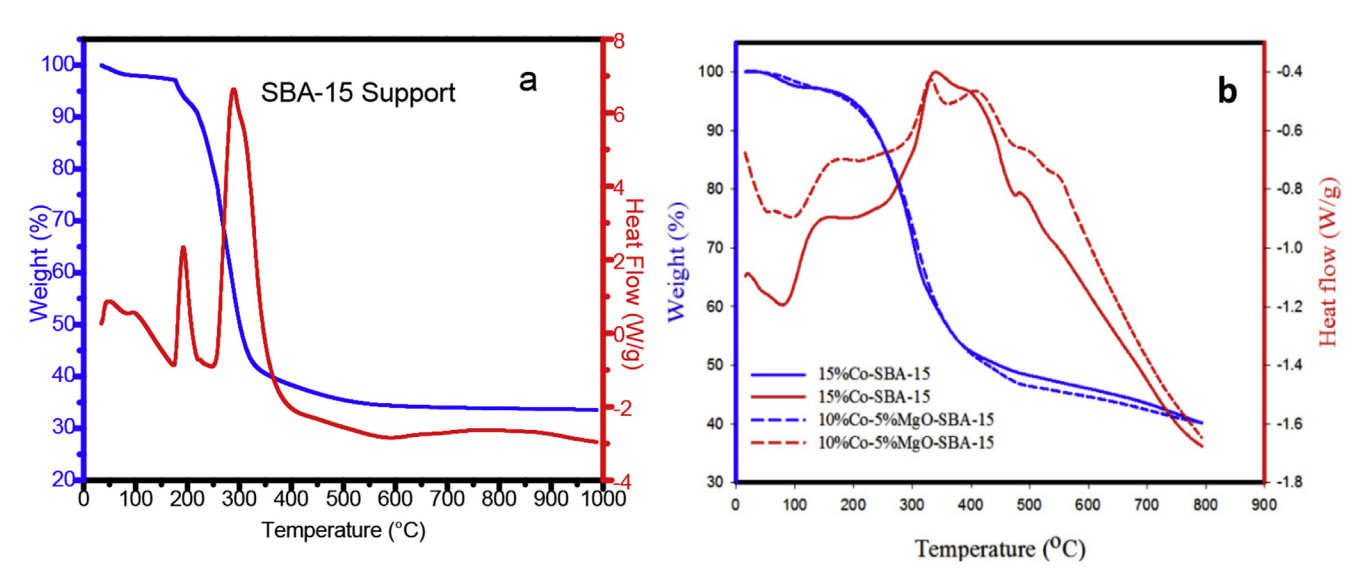


Fig. 1 - TGA-DSC profiles of as-prepared (a) SBA-15 (b) 15%Co-SBA-15 and 10%Co-5%MgO-SBA-15 recorded in air.

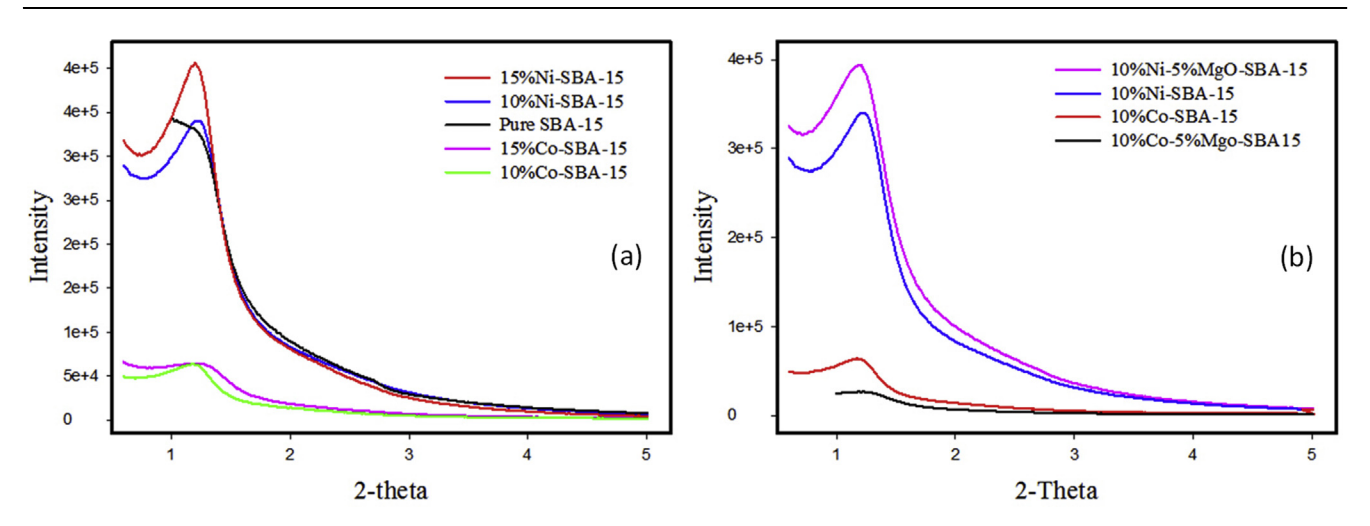


Fig. 2 - Small angle XRD patterns of different SBA-15 based catalysts.

presence of peaks between 1° and 2°-theta indicates that all the materials possessed ordered mesoporous structures. However, the high intensity of the SBA-15 support and the nickel-based catalysts underpinned the fact that those samples had a long range ordered mesoporous structure and better pore periodicity. This ordered trend is supported by the slightly higher surface areas of the Ni-based catalysts in Table 4. The very low peak intensity of 10%Co-5%MgO-SBA-15 in Fig. 2b suggests its least ordered framework. The IMPG catalyst did not show any low angle reflections at all.

The wide-angle X-ray diffraction (WXRD) patterns of different Ni/Co/MgO based SBA-15 catalysts are presented in Fig. 3. The WXRD spectra of 10%Co-SBA-15, 15%Co-SBA-15, and 10%Co-5%MgO-SBA-15 showed five peaks at 2-theta of 31.3°, 36.8°, 45°, 59.0°, and 64.8° corresponding to the planes (220), (311), (511) and (440) of the cubic phase of Co_3O_4 , respectively (JCPDS# 76-1802) [34,35]. The diffraction peak of MgO that usually occurs at a 2-theta of 42° was not detected for 10%Co-5%MgO-SBA-15 catalyst, suggesting that MgO

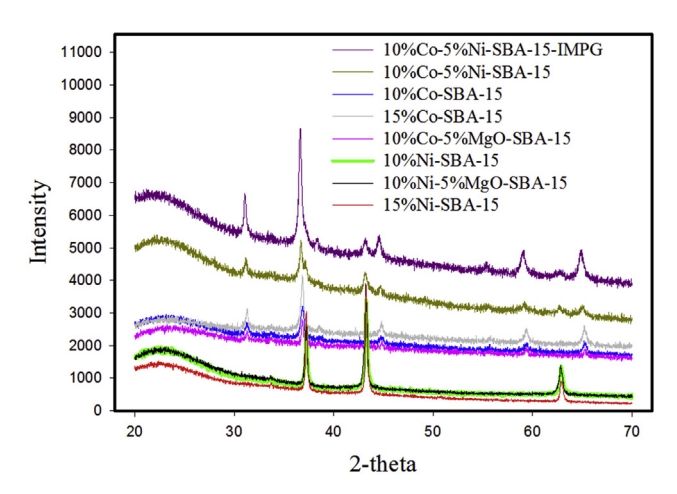


Fig. 3 — WXRD patterns of different Ni/Co/MgO based SBA-15 catalysts with 10–15 wt% metal loading.

diffractions are either masked by the crystallinity of the cobalt oxide crystallites or may be highly dispersed in SBA-15 [36]. The WXRD spectra of 10%Ni-SBA-15, 15%Ni-SBA-15, and 10% Ni-5%MgO-SBA-15 catalysts displayed peaks at 2-theta = 37.3°, 43.3°, and 62.9° that can be assigned to the (111), (200) and (220) planes of the cubic NiO (JCPDS# 78-0643), respectively [37]. Once again, no peak related to MgO was noticed in the 10%Ni-5%MgO-SBA-15 catalyst.

In contrast to monometallic-SBA-15, the WXRD patterns of bimetallic 10%Co–5%Ni-SBA-15 and 10%Co–5%Ni-SBA-15-IMPG displayed four diffraction peaks observed at 2-theta = 31.3°, 36.8°, 59.0°, and 64.8° corresponding to (220), (311), (511), and (440) planes respectively, indicating the formation of cobalt oxide (Co₃O₄) [35]. There is another noticeable peak at 2-theta = 43.3°, which is assigned to (200) plane of cubic NiO (JCPDS# 78-0643). Also, the peak observed at 2-theta = 43.4°, assigned to (400) plane, suggests the formation of the nickel—cobalt oxide (NiCo₂O₄) spinel polymorph [29]. The oxide crystallite sizes and the actual metal loadings (weight percent) determined using ICP-OES are shown in Table 1. The actual metal loadings compared fairly well with the intended loadings. The actual metal loading in SBA-15

Table 1 — Summary of ICP-OES metal loading and XRD metal oxides crystal size.						
Intended Catalyst Loading	Actual metal loading (wt %) ICP-OES	Metal crystal size (nm)				
Pure SBA-15	0	0				
10%Co-SBA-15	8.2	22.29				
15%Co-SBA-15	12.52	26.72				
10%Co-5%MgO-SBA-15	Co-5.2	43.43				
10%Ni-SBA-15	8.6	31.44				
15%Ni-SBA-15	Ni-12.24	35.38				
10%Ni-5%MgO-SBA-15	Ni-7.3	31.83				
10%Co-5%Ni-SBA-15	Co-6.45, Ni-2.82	26.43				
10%Co-5%Ni-SBA-15-IMPG	Co-5.77, Ni-2.65	26.2				

usually plays a significant role in the catalyst's activities [38]. The sizes of the metallic oxide crystallites ranged from 22 nm to 43nm.

N_2 -Physiosorption analysis to study textural properties of M-SBA-15

The N₂ adsorption-desorption isotherms and pore size distribution (PSD) for calcined SBA-15 samples are shown in Fig. 4a and b respectively. All the isotherms represent the type IV isotherms which is considered typical for solid mesoporous materials based on IUPAC classification [39]. Each plot of Fig. 4 (a) can be divided into three different regions: The first region is linear which can be attributed to the monolayer adsorption that occurs at low relative pressure ($P/P_0 = 0-0.4$), followed by the second steep region resulting from capillary condensation within the mesopores that occurred at an intermediate pressure ($P/P_0 = 0.4-0.7$), and finally, the third region at pressure $(P/P_0 = 0.4-1)$ can be attributed to multilayer adsorption of the N2. All the samples in Fig. 4 (a) exhibited H1 type hysteresis loop that corresponds to the 2-D cylindrical shaped pores of SBA-15. Properties such as surface areas, pore sizes, and pore volumes of different Co/Ni/MgO based SBA-15 catalysts obtained from N2 adsorption/desorption experiments are summarized in Table 4. The surface area of the catalysts ranged from 565.7 to 742.2 m²/g, pore diameter from 4.76 to 5.88 nm, and a pore volume between 0.68 cm³/g and 0.93 cm³/g. The wide range of the values is attributed to the differences in the type and weight percent of the metals in the SBA-15 framework. Generally, addition of MgO to the SBA-15 support as well as increase in the metal (Co & Ni) loading from 10% to 15% caused a decline in the surface area. This trend is due to the mesopores of the silica framework being partially filled with these metal oxides which decreases the total pore volume and hence the surface area of the catalyst. When different synthesis methods were considered, 10%Co -5%Ni-SBA-15 prepared by one-pot method showed higher surface area, but lower pore volume and diameter compared to that of 10%

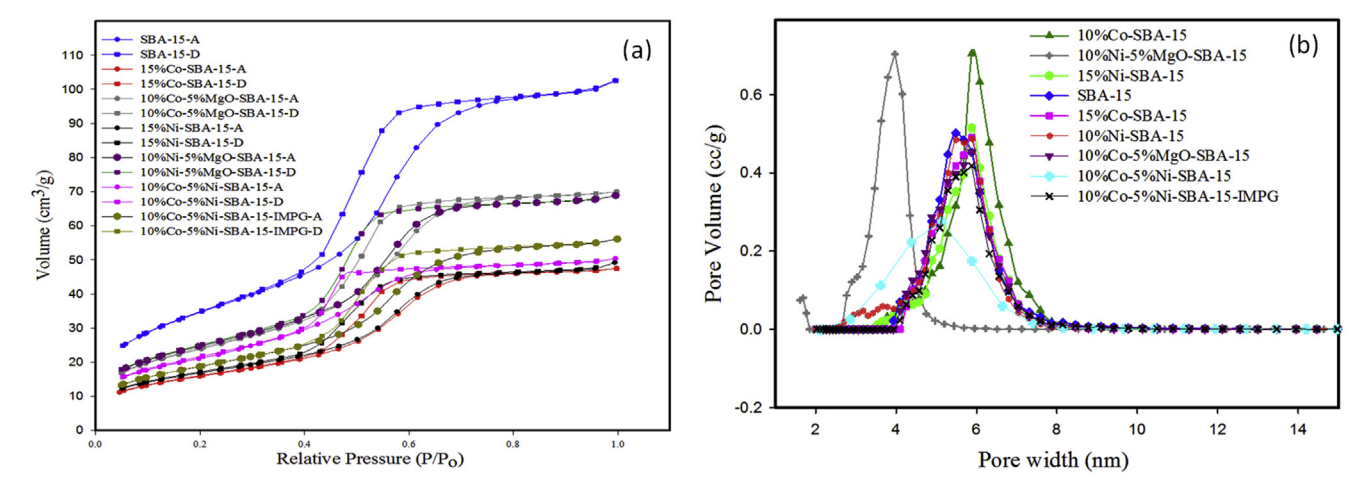


Fig. 4 - (a) N₂ adsorption-desorption isotherms for SBA-15 and metal incorporated SBA-15 catalysts and (b) pore size distribution of different samples.

Co-5%Ni-SBA-15-IMPG which was prepared by impregnation. Depending on the type of metal, PSD of all catalysts varied from about 2.5 nm to 8 nm which is within the mesoporous domain of porous frameworks.

SEM-EDX elemental mapping and TEM imaging

Fig. 5 (a) shows the SEM spectrum confirming the presence of the elements and (b) EDX-ray reflections of the functionalized metals in the silica support. The SBA-15 and Ni/Co/MgO based SBA-15 catalyst were also studied by transmission electron microscopy (TEM). Fig. 6 confirms that both materials are mesoporous over a wide area.

Temperature programmed reduction (TPR) analysis of SBA-15 supported catalysts

The TPR studies were done to understand the nature of the interactions between the metal species and SBA-15 support, and how the interactions affected metal oxide reducibility as well as their GSR activity. The TPR of different Ni/Co/MgO based SBA-15 catalysts is shown in Fig. 7. The profile of the 15%Co-SBA-15 catalyst shown in Fig. 7a displayed two recognizable reduction peaks. The first reduction peak around 304 °C is due to the reduction of Co₃O₄ to Co_O. The reduction of Co_O to metallic Co resulted in the second reduction peak centered at about 485 °C. These results agreed with the findings of both Luisetti et al. and Tang et al. [40,41]. The TPR profile of the 10%Co–5%MgO-SBA-15 shown in Fig. 7 (a)

displayed two continuous reduction peaks. The first reduction peak at 350 °C is attributed to the reduction of Co₃O₄. Incorporation of MgO did not seem to improve the reducibility of the cobalt oxides but interacted strongly with the cobalt (II) oxides resulting in elimination of the intermediate reduction step of CoO to metallic Co observed in 15%Co-SBA-15. This implies that the second reduction peak at 850 °C is possibly due to the presence of spinel Mg-silicate or Co-silicate species formed during the calcination process [42]. Fig. 7 (b) shows a sharp reduction of bulk nickel oxide at about 393 °C in the TPR profile of 15%Ni-SBA-15 and it is consistent with findings reported by Afzal et al. [43]. In the 10%Ni-5%MgO-SBA-15 catalyst, the reduction peak at 385 $^{\circ}\text{C}$ is also attributed to the reduction of NiO to Ni metal. From the reduction profiles of 10%Ni-5%MgO-SBA-15 and 15%Ni-SBA-15, the addition of MgO to 15%Ni-SBA-15 did not yield any noticeable decrease in the reduction temperature of the supported NiO crystallites.

Fig. 7c shows the TPR profile of one-pot and impregnated 10%Co-10%Ni-SBA-15 catalysts. Although NiO is reduced at 393 °C in 15%Ni-SBA-15, for 10%Co-5%Ni-SBA-15, prepared by one-pot procedure, reduction of NiO occurred at around 296 °C. The addition of cobalt lowered the reduction temperature of NiO by roughly 100 °C, thus reducing the total activation energy of the catalyst and improving its activity as observed in Section on GSR Studies with One-pot versus Impregnated Bimetallic Catalysts. This observation is similar to that of Zhao et al. who reported that SBA-15 supported bimetallic Ni—Co catalyst is more easily reduced than the monometallic species [29]. For the one-pot bimetallic catalyst,

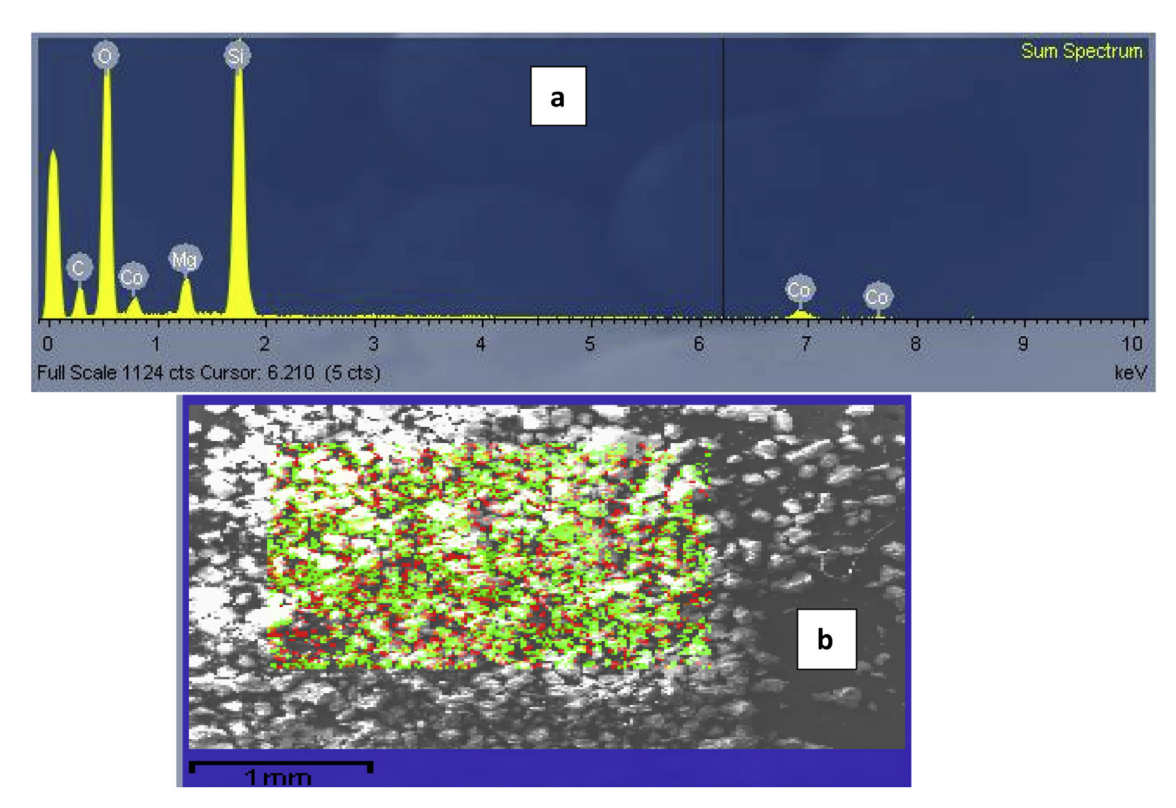


Fig. 5 - (a) SEM Spectrum of 10Co-5MgO-SBA-15 and (b) SEM Image of active sites (Mg-green) and (Cobalt-red) on SBA-15 support-white.

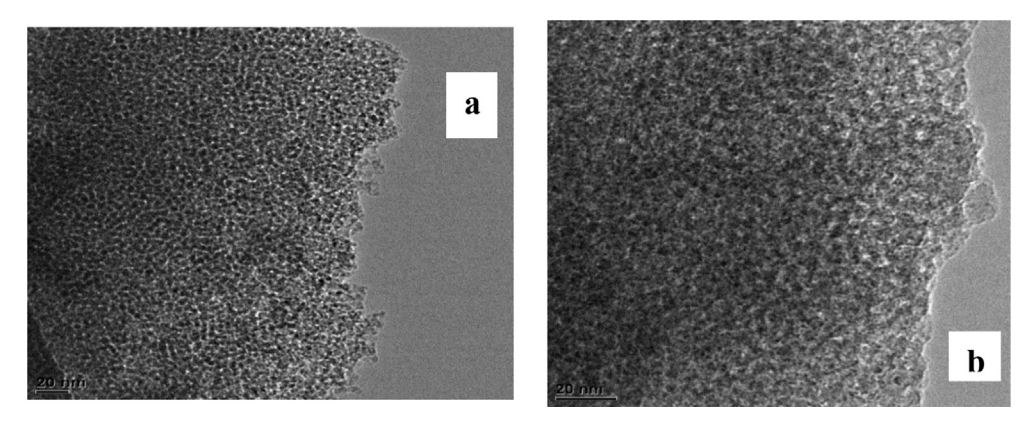


Fig. 6 – TEM images of (a) mesoporous-SBA-15 (b) 10%Co-5%Ni-SBA-15 catalysts.

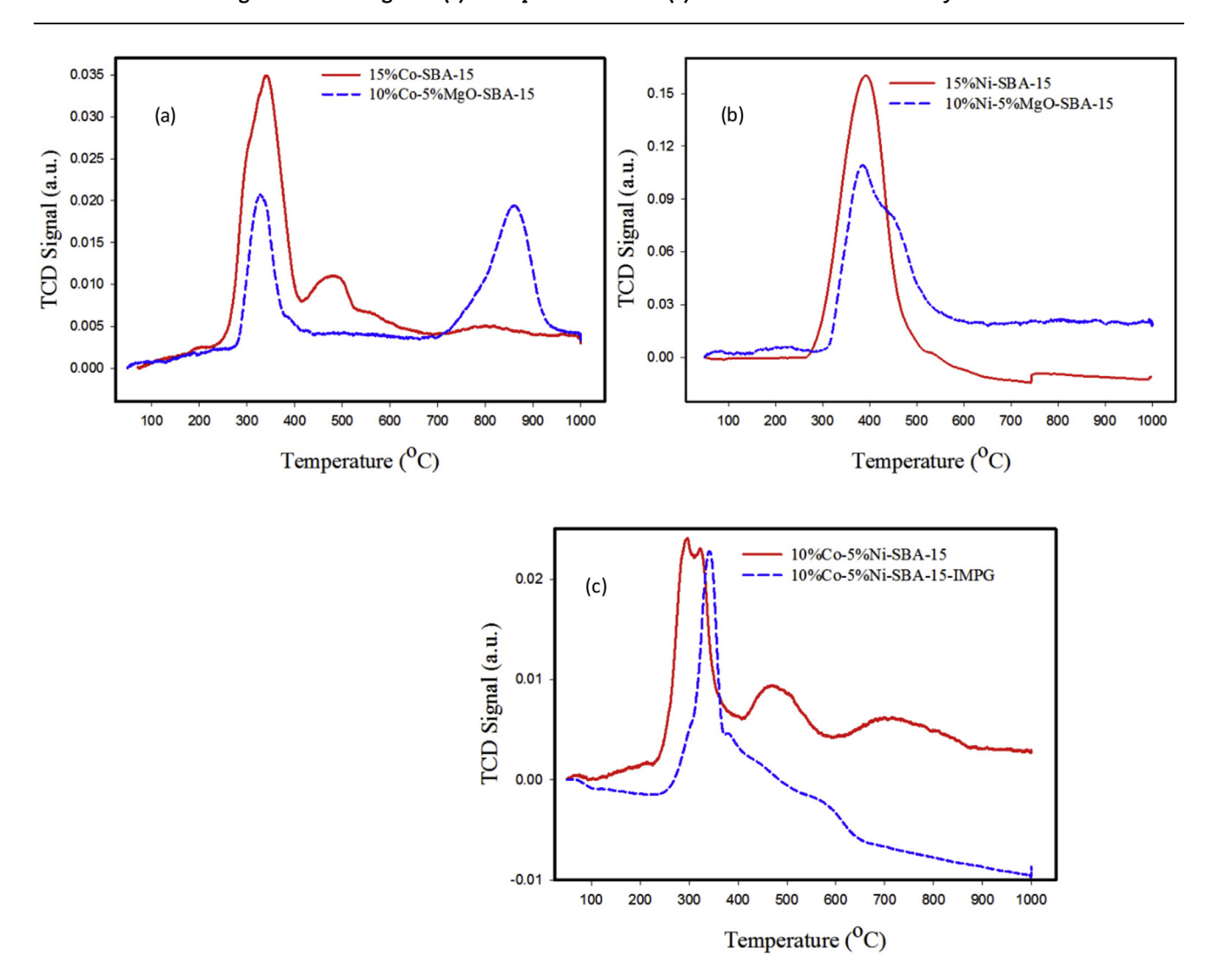


Fig. 7 – TPR profiles of (a) 15%Co-SBA-15 and 10%Co-5%MgO-SBA-15, (b) 15%Ni-SBA-15 and 10%Ni-5%MgO-SBA-15, (c) 10% Co-5%Ni-SBA-15 and 10%Co-5%Ni-SBA-15-IMPG.

the emergence of peak at 469 $^{\circ}$ C could be due to the reduction of CoO, and the third peak in the range of 600–900 $^{\circ}$ C could be due to the reduction of spinel NiCo₂O₄ (nickel cobaltite) crystal structures which are usually very difficult to reduce [44].

Similarly, the bimetallic 10%Co-5%Ni-SBA-15-IMPG catalyst displayed a peak around 342 °C which corresponds toreduction of NiO, and the second high temperature reduction peak between 500 and 600 °C is most likely due to reduction of

 Co^{3+} , Co^{2+} and Ni^{2+} ions located at the tetrahedral and octahedral sites of the spinel NiCo_2O_4 ternary crystal phases [45,46].

Results and discussion

Six different catalysts, each having a total metal loading of 15 wt%, were tested for GSR activity studies. The effect of temperature (450 °C–700 °C) on glycerol conversion and selectivity of $\rm H_2$, CO, CH₄, and CO₂ products are reported in Table 2. Results from all catalysts showed that glycerol conversion increased with increase in temperature up to 700 °C. Preliminary GSR reactions were performed with all catalysts; based on each catalyst's ability to bolster glycerol conversion, stability and hydrogen selectivity, as well as tendency to produce minimal undesired byproducts (CO, CH₄ & CO₂), 650 °C was selected as the optimum temperature under our reaction conditions. In general, low glycerol conversion accompanied by high CO selectivity and low $\rm H_2$ selectivity were obtained at 450 °C; these results are similar to the findings of Zhang et al. [17].

Co-based catalysts

Based on our experimental results, cobalt is not a low temperature GSR catalyst because glycerol conversion was negligible, 4.3% at 450 °C, suggesting that about 96% of glycerol did not react (or unconverted) at this temperature. However, a 100 °C rise in temperature to 550 °C for 15%Co-SBA-15 yielded an impressive 92% conversion and about 87% hydrogen selectivity. With further increase in temperature to 650 °C and 700 °C, glycerol conversion increased to a maximum of 96%

while hydrogen selectivity decreased to ~79% and 61% at $650\,^{\circ}\text{C}$ and $700\,^{\circ}\text{C}$, respectively.

Addition of MgO to Co-SBA-15 (10%Co-5%MgO-SBA-15) significantly enhanced glycerol conversion from ~10% at 450 °C to 100% at 700 °C. Hydrogen selectivity held fairly steady but CO2 selectivity particularly at 550 °C and 650 °C decreased by ~30% in the MgO modified catalyst. This observation buttressed our hypothesis that MgO avails strong basic active sites that decrease coking and CO2 production via a Lewis acid-base (i.e. CO2 acts as the lewis acid) mechanism to prolong and improve the catalyst activity. Although CO selectivity remained fairly the same, CH₄ production also decreased ~50%. As mentioned in our TPR studies in Section of Temperature programmed reduction (TPR) analysis of SBA-15 supported catalysts, interaction of MgO with cobalt oxides enhanced the reduction of Co₃O₄ straight to the active Co metal without going through the transitional Co₃O₄ to CoO phase. This lower activation energy path compared to that of the unmodified Co-SBA-15 catalyst most likely played a positive role in the better GSR performance of the modified catalyst.

Ni-based catalysts

In contrast to cobalt, nickel catalysts performed much better at lower temperature. At 450 °C, 15%Ni-SBA-15 yielded ~50% glycerol conversion, 38% $\rm H_2$, while 10%Ni-5%MgO-SBA-15 yielded ~25% conversion with 52% selectivity to $\rm H_2$. As in the case of cobalt, MgO modified Ni catalysts generally reduced the CO $_2$ selectivity by ~30% except at 700 °C. However, in terms of glycerol conversion, the activity of the MgO modified and unmodified Ni catalysts were similar between 550 °C and 700 °C indicating that MgO as a promoter bolstered cobalt

Catalyst ID	Temperature (°C)	Conversion (%)	Selectivity (%)			
			H ₂	CO	CH ₄	CO
15% Co-SBA-15	450	4.3	39.7	67.7	7.3	25.0
	550	92.0	86.8	12.0	7.1	80.9
	650	96.2	78.8	16.0	11.7	72.3
	700	96.5	61.4	47.5	9.5	43.0
15%Ni-SBA-15	450	51.5	38.3	64.3	16.4	19.3
	550	78.3	74.3	31.5	6.8	61.7
	650	85.6	82.7	21.4	6.5	72.3
	700	89.1	70.8	47.0	9.7	43.3
10%Co-5%Ni-SBA-15	450	50.5	63.4	42.5	5.0	52.
	550	84.6	77.2	17.9	9.5	72.
	650	100.0	80.0	17.8	7.6	74.
	700	100.0	73.6	19.7	9.6	70.
.0%Co-5%Ni-SBA-15-IMPG	450	69.9	62.6	48.7	7.8	43.
	550	89.8	81.1	13.2	7.6	79.
	650	100.0	82.8	15.1	5.7	79.:
	700	100.0	79.1	14.2	7.8	78.
0%Co-5%MgO-SBA-15	450	10.9	13.6	60.5	3.5	36.
·	550	94.4	72.6	36.1	5.2	58.
	650	99.0	72.6	44.2	4.0	51.
	700	100.0	68.6	47.5	4.9	47.
.0%Ni-5%MgO-SBA-15	450	24.9	52.0	62.1	7.3	30.
	550	64.0	59.8	52.0	7.3	40.
	650	80.7	69.8	43.8	5.3	50.
	700	85.5	59.7	48.9	6.6	44.

activity but had negligible effect on the activity of nickel catalysts. It must be pointed out that despite the better lower temperature activity by nickel catalysts, cobalt catalyst, exhibited superior and more impressive GSR activity than nickel in terms of glycerol conversion and H₂ selectivity, particularly at the optimum temperature of 650 °C. Our observed trend concurs with the studies of Carrero et al. who reported that maximum value of glycerol conversion (92%) was reached after 5 h at 600 °C and WHSV of 7.7 h⁻¹ [47,48]. Similarly, Zamzuri and coworkers demonstrated that addition of basic promoters like MgO to several nickel supported catalysts in glycerol steam reforming significantly reduced the amount and rate of carbon deposition on the Ni-active sites and ultimately bolstered the stability and shelve-life of the catalysts [49].

GSR studies with one-pot versus impregnated bimetallic catalysts

Bimetallic catalysts prepared by one-pot method (10%Co-5% Ni-SBA-15) and incipient wetness impregnation (10%Co-5% Ni-SBA-15-IMPG) exhibited remarkable GSR activity compared to the monometallic species. At high temperature 650 °C and 700 °C, both the one-pot and impregnated catalysts showed similar activity by attaining 100% glycerol conversion at steady state. However, at low temperature of 450 °C, although both yielded ~62% H₂ selectivity, the one-pot catalysts showed 50% glycerol conversion compared to ~70% by the impregnated catalyst. This low temperature superiority of the IMPG catalyst over the one-pot was most likely due to the differences in the synthesis procedure of the catalysts. The one-pot bimetallic catalyst has slightly smaller pore diameter than the IMPG (Table 4) catalyst and possessed long-range ordered mesopores (Section X-ray diffraction of different M-SBA-15 and ICPOES analysis of catalysts-SXRD) whereas the IMPG showed no ordered morphology. At lower temperature, the average molecular velocity, kinetic energy and mass diffusion of the reactant molecules are minimized. Hence the one-pot "cage-like" ordered framework becomes an additional miniature barrier to retard diffusion of the glycerol-water molecules, limiting their interaction with the active sites which results in a much lower conversion. However, at high temperature, the reactant molecules obtain the threshold kinetic energy needed for maximum mass diffusivity through the pores which consequently overcome the diffusion barrier. Hence, the glycerol conversion obtained from catalysts prepared by both methods is similar at high temperature (650 °C and 700 °C). Of all the studied catalysts, the bimetallic catalysts produced the least CO and highest CO2 selectivity signifying that both bimetallic species favored the water-gas shift reaction and hence abated CO poisoning-the most probable reason for the dominant GSR inactivity. This superior GSR performance could also be ascribed to a synergistic interaction between the Co and Ni metal oxides in terms of reduced selectivity towards undesired products. This synergism is observed in the TPR studies (Section on Temperature programmed reduction (TPR) analysis of SBA-15 supported catalysts) which showed that Co enhanced the reducibility of NiO in the silica framework. Also, a careful analysis of Table 1 reveals that the addition of Co reduced the NiO crystallite

sizes from 31 nm to 35 nm to an average of 26 nm in the bimetallic species. This reduction, approximately 20% in particle sizes likely enhanced the distribution of the active metal sites thereby improving the catalytic activity. Our inference is corroborated by the studies of Zhao and coworkers [50] as well as other researchers [51], who elucidated on the synergistic propensity of Co and Ni bimetallic systems to resist coking thereby improving activity and selectivity of desired products. In summary, based on our reaction parameters, we ascertained that the GSR activity was in the order: $10\%\text{Co}-5\%\text{Ni-MPG} \geq 10\%\text{Co}-5\%\text{Ni-SBA-15} > 10\%\text{Co}-5\%\text{MgO-SBA-15} > 15\%\text{Co-SBA-15} > 15\%\text{Ni-SBA-15} > 10\%\text{Ni-5}\%\text{MgO-SBA-15}.$

GSR - catalyst long-term performance studies

Long-term stability of the catalysts shown in Table 2 was investigated for continuous 40 h at 650 °C with GHSV of 2200 h^{−1} to evaluate their relative ability to resist deactivation and to have a better understanding of the factors that initiate/ cause the deactivation process. The spent catalysts were further characterized by powder XRD, BET and TGAtemperature programmed oxidation (TPO) to determine any morphological and physiochemical changes that may have occurred during the entire 40 h and how the changes may have impacted the performance of the catalysts. Glycerol conversion and selectivity of the reformate gases after 40 hrs are compared in Fig. 8. Generally, with the exception of 15%Ni-SBA-15, all the other catalyst showed consistent stability and 90-100% glycerol conversion. Particularly, the bimetallic catalysts maintained 100% glycerol conversion with no sign of deactivation for 40 hrs. However, 15%Ni-SBA-15 showed ~85% conversion only for the first 8 hrs and then declined sharply to ~10% at the end of the reaction. We were intrigued by this quick loss of activity and repeated the GSR reaction three times with 15%Ni-SBA-15 only to obtain the same results each time. The possible causes of this poor GSR activity are explained in sections 3.7.1 & 3.7.2. In contrast, addition of 5% MgO to 10%Ni-SBA-15 (i.e. 10%Ni-5%MgO-SBA-15) prolonged the 85% conversion until approximately 28 h and then only decreased to 80% at the end of 40 h.

In terms of the reformate gases selectivity, 15%Ni-SBA-15 was once again the outlier. At the end of 40 hrs, each catalyst showed \sim 70%–80% H_2 selectivity while 15%Ni-SBA-15 alone yielded only 40% H2 as well as the highest quantity of undesired byproducts CO and CO₂. A careful examination of Fig. 8 revealed that in the case of 15%Ni-SBA-15, as the H₂ and CO₂ selectivity decreased, the CO selectivity increased significantly suggesting that the monometallic 15%Ni-SBA-15 favored the reverse water-gas shift reaction and hence more vulnerable to CO poisoning. Junjie Chen et al. [52] as well as Li. Shuirong and coworkers [53] also confirmed that nickel catalysts do not promote the water gas shift reaction. Calles et al. [54] also noticed a similar trend for GSR activity studies with Ni-SBA-15 wherein they inferred that glycerol conversion sharply decreased to 46% just after 5 hrs. However, they found that Ni promoted catalysts (Ni-Mg-SBA-15 and Ni-Ca-SBA-15) showed an average of 97% glycerol conversion after 5 hrs. Their findings firmly underscore the performance enhancing effect of MgO addition we noticed in Section of Ni Based Catalysts. Additionally, for the first 20 hrs the observed

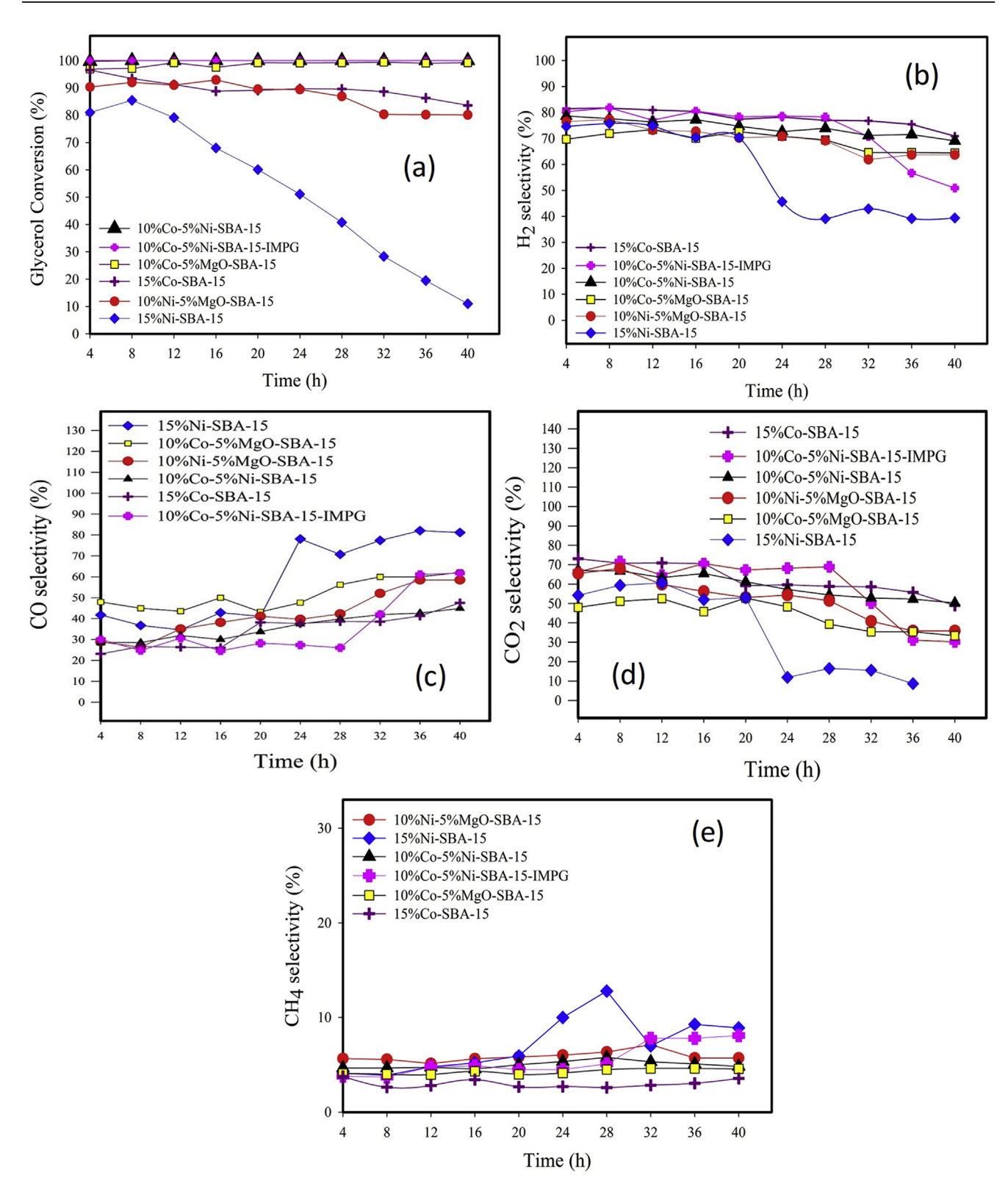


Fig. 8 – (a) Glycerol conversion (b) H_2 selectivity (c) CO selectivity (d) CO_2 selectivity (e) CH_4 selectivity patterns for catalysts at 650 °C with water: glycerol molar ratio of 12:1 and GHSV of 2200 h^{-1} .

selectivity of CO and $\mathrm{CH_4}$ for 15%Ni-SBA-15 were about 40%, and 6% respectively and augmented to about 81% and 9% respectively after 40 h further confirming the specificity of Nickel for CO gas. Overall, our results indicate that cobalt-

based catalysts are superior in stability and catalytic GSR activity compared to nickel-based catalysts. Addition of MgO increased the $\rm H_2$ selectivity of 15%Ni-SBA-15 and improved the catalyst stability by inhibiting carbon formation and CO

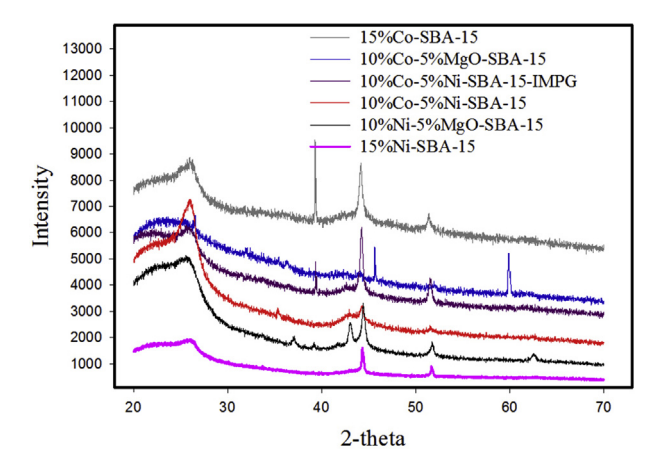


Fig. 9 – Wide angle XRD patterns of different metal incorporated SBA-15 catalysts after 40 h of GSR studies.

poisoning as well as assisting in the steam oxidative elimination of coke. Our determination of the extreme vulnerability of Ni catalysts to CO and carbon poisoning have been elucidated by other researchers. Denis et al. [25] inferred that although Ni-catalysts are generally susceptible to carbon monoxide and coke poisoning, tailoring specific supports and addition of alkali metal promoters like Na reduces the dehydration of the carbonaceous feedstock e.g. ethanol/ethylene and thereby reducing coking effects substantially. Papageridis et al. [24] also observed that during GSR with alumina supported Cu, Ni and Co catalysts, Ni/Al displayed the best glycerol conversion. However, Co/Al and Cu/Al were much more stable and deactivated slowly compared to the Ni-catalyst that showed a very sharp drop in activity during the first 7 h.

XRD of spent catalysts

The wide-angle X-ray diffraction of Co/Ni/MgO based SBA-15 spent catalysts after 40 h on-stream are represented in Fig. 9. Compared to the WXRD pattern in Fig. 3, new peaks emerged after 40 h for both the mono-and bimetallic catalysts.

These peaks around $2\theta=26^\circ$, 43.7° , and 53° correspond to the planes (002), (100), and (004) are reported to be characteristic diffraction patterns of carbon/coke residues [37,55]. 10% Co–5%Ni-SBA-15 catalyst, after 40 h on-stream studies, has a weak peak around $2\theta=43.4^\circ$ that is assigned to the (200) plane of NiO. 10%Co5%-Ni-SBA-15-IMPG showed a sharp peak at $2\theta=37^\circ$ that corresponds also to the presence of NiO [56].

TGA-TPO analysis of spent catalysts

The temperature program oxidation (TPO) analysis was performed with TGA to measure the extent of carbon accumulation on the active sites of the metals after continuous 40 hrs of $\rm H_2$ production.

In Fig. 10, the TGA-TPO profiles of 10%Ni-5%MgO-SBA-15 and 15%Ni-SBA-15 spent catalysts are shown as prototypes of the coking effect after 40 h on-stream studies. The thermograms of the other catalysts are shown in Fig. 11 (Supplemental) and their percent carbon deposition is quantified in Table 3 under typical reaction conditions. The thermal profile showed a substantial amount of carbon oxidation in the 450 °C-625 °C temperature range. 10%Ni-5%MgO-SBA-15 catalyst exhibited an exothermic heat loss centered at 550 °C which is due to oxidative removal of amorphous carbon. In the case of 15%Ni-SBA-15, the peak at 650 °C is typically ascribed to graphitic carbon deposits which are characteristically obdurate and very difficult to remove from the active sites. Our results are consistent with the findings of Calles et al. [37] and Choong's group [57] for similar studies. They reported that the amorphous carbon oxidizes between 400 and 550 °C, and the more crystalline graphitic carbon oxidizes above 600 °C. As shown in Table 3, MgO promoted catalysts exhibited a much lower affinity for carbon. For example, 68.5% coking was determined for 15%Co-SBA-15 and 28.5% for 10%Co-5%MgO-SBA-15. This suggests that addition of 5%MgO reduced the amount of carbon dioxide or carbon deposition on the metal active sites by 58%. Similarly, addition of 5% MgO to Ni-SBA-15 reduced the coking effect by approximately 40%. The correlation between the coking depletion ability of MgO and

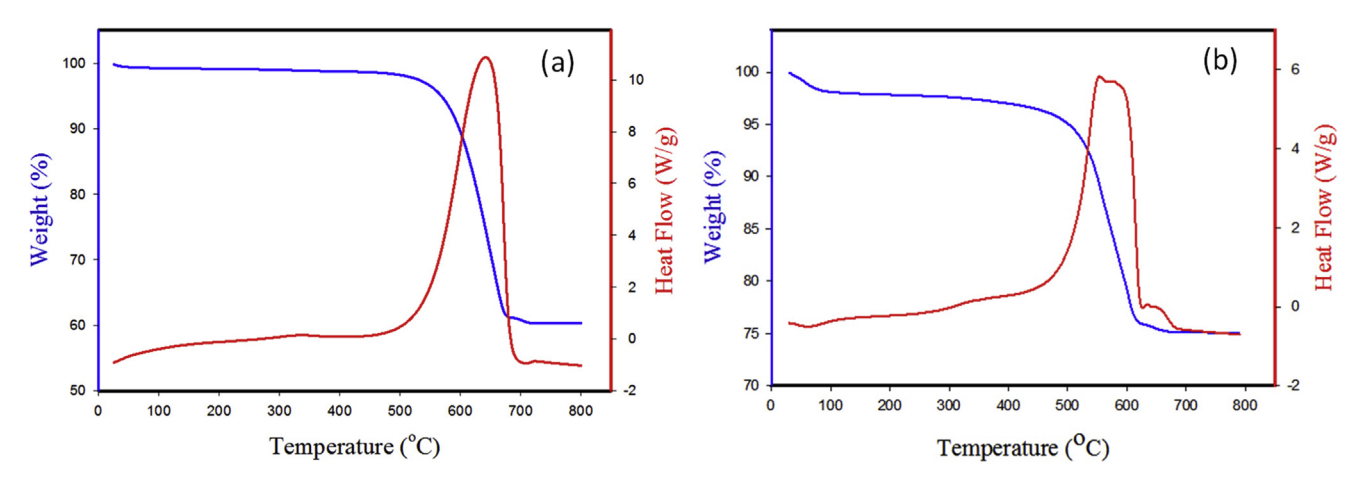


Fig. 10 - Themograms of Spent (a) 15%Ni-SBA-15 (b) 10%Ni-5%MgO-SBA-15 catalysts after GSR reaction for 40 h.

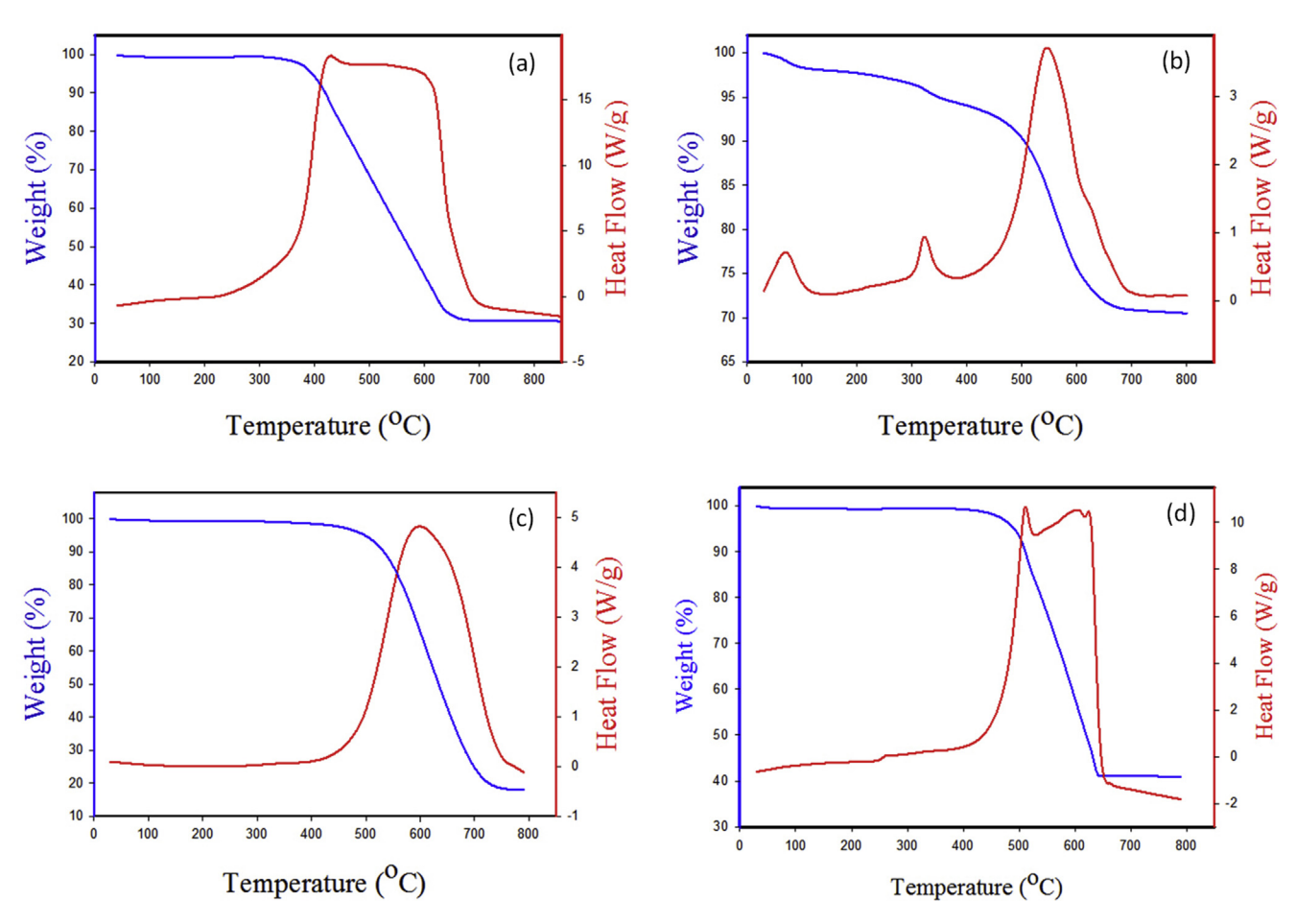


Fig. 11 — Thermograms of spent catalysts after 40 h GSR (a) Co-SBA-15 (b) Co-MgO-SBA-15 (c) Co-Ni-SBA-15 (one pot) (d) Co-Ni-SBA-15 (Impregnation).

Table 3 $-$ Quantitative evaluation of coke residues on the active site of catalysts after 40 h on-stream studies with different catalysts.						
Catalyst ID	15%Co-SBA-15	15%Ni-SBA-15	10%Co-5%MgO- SBA-15	10%Ni-5%MgO- SBA-15	10%Co-5%Ni- SBA-15	10%Co-5%Ni- SBA-15-IMPG
Weight loss (%) due to carbon oxidation	68.5	38.4	28.5	23	81.3	53

glycerol conversion as well as stability of the catalysts can be clearly seen in Fig. 8. In terms of catalyst stability, effect of the MgO promotion was very pronounced with the Ni catalysts. While 10%Ni-5%MgO-SBA-15 maintained ~90% glycerol conversion for the entire 40 h, Ni-SBA-15 showed a precipitous steady decline in conversion and stability just after 8 h onstream and only 10% glycerol conversion after 40 hrs.

In the case of the bimetallic catalysts, the one-pot method yielded a significant 81% carbon deposition relative to 53% of the catalysts prepared by the impregnation approach. The method of catalyst preparation seems to control the metal-support interaction and stereochemistry of the active sites making some active sites more prone/susceptible to deposition than others. Choong et al. reported that alkaline earth metals (like calcium) as catalyst promoters, produce less

amount of coke by activating H_2O adsorption on the catalyst surface, thereby enhancing the steam gasification of coke [57].

BET of spent catalysts

All the spent catalysts were cooled to room temperature in the presence of N_2 after GSR activity studies and re-calcined in air at 625 °C to remove carbon deposits and then used to determine the actual decrease in surface area after 40 h. Complete removal of all surface carbon deposits was confirmed by direct injection of CO_2/CO (emanating from the oxidation of carbon) in the GC until no more CO_2/CO peaks were detected.

Fig. 12 (supplemental) shows that the N_2 adsorption-desorption isotherms are skewed (no more Type (IV) isotherms and somewhat flattened compare to the isotherms of

Table 4 $-$ Textural properties of calcined versus spent catalysts.							
SBA-15 Supported Catalysts	Surface Area ^a (m ^b /g)	Surface Area ^a (m ^b /g) after 40 h Reaction	Pore Size ^b (nm)	Pore Size ^b (nm) after 40 h Reaction	Pore Volume ^c (cm ^c /g)	Pore Volume ^c (cm ^c /g) after 40 h Reaction	
Pure SBA-15	703.93	_	5.07	_	0.89	-	
10%Co-SBA-15	742.17	-	5.88	-	0.93	-	
15%Co-SBA-15	628.78	166.29	5.12	9.07	0.81	0.38	
10%Co-5%MgO-SBA-15	647.02	288.60	4.95	5.51	0.8	0.39	
10%Ni-SBA-15	758.98	-	5.86	_	0.94	-	
15%Ni-SBA-15	596.52	173.04	5.19	8.56	0.77	0.37	
10%Ni-5%MgO-SBA-15	707.33	313.70	4.76	5.52	0.82	0.43	
10%Co-5%Ni-SBA-15	706.57	260.20	4.89	6.48	0.68	0.42	
10%Co-5%Ni-SBA-15-IMPG	565.7	191.18	5.13	8.34	0.72	0.39	

^a Variation range ±2%.

^c Variation range ±2%.

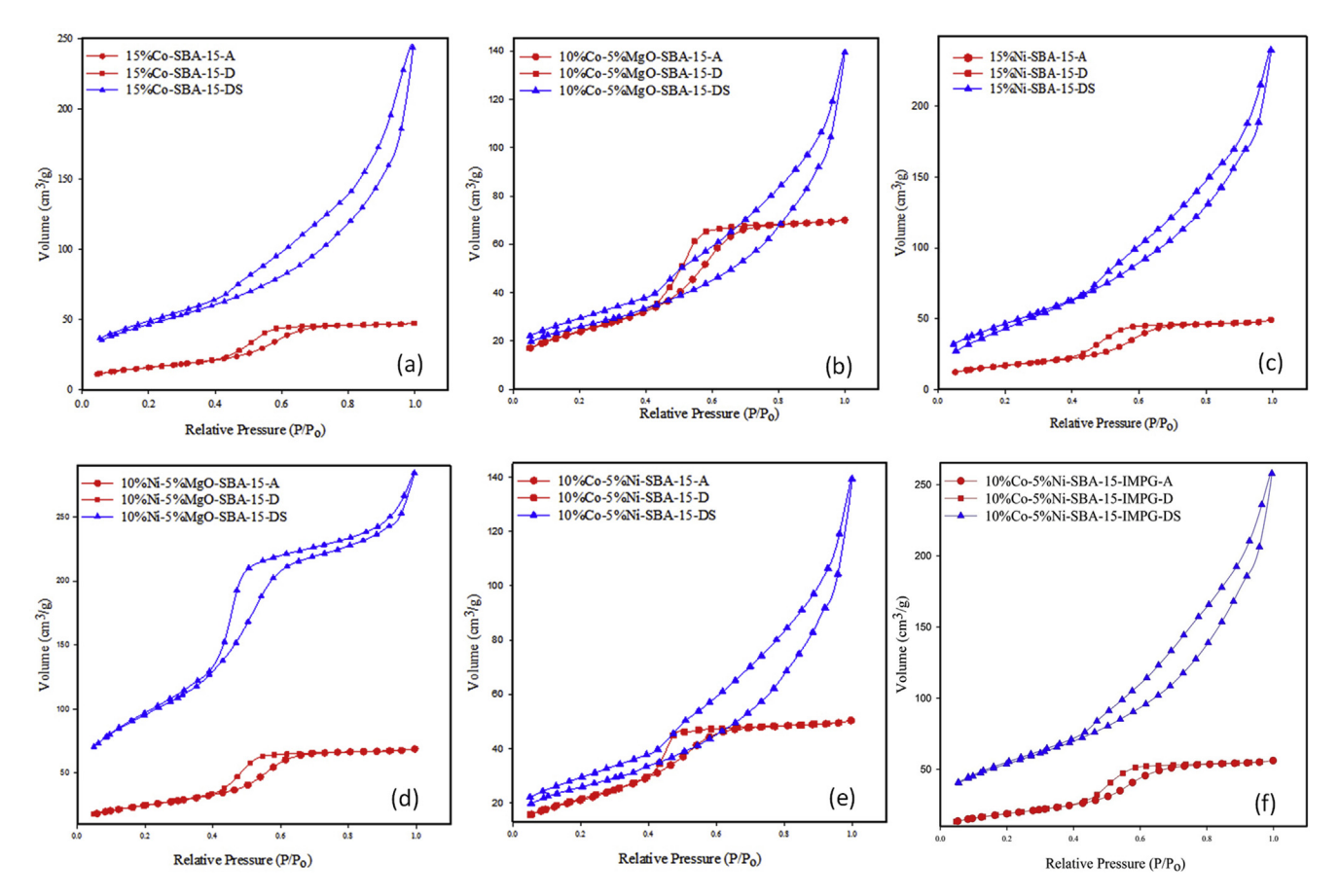


Fig. 12 - N₂ adsorption-desorption isotherms of spent SBA-15 catalysts after 40 h GSR.

the unspent catalysts in Fig. 4a. This suggests a significant loss of the well-defined mesoporosity and structural integrity of the catalysts compared to the original samples [58].

Table 4 unambiguously confirms that after 40 h on-stream all the catalysts lost quite a significant amount of the total surface area indicating some degree of hydrothermal structural disintegration. Prior to all reactions, the average surface area of all the unspent catalysts was approximately 640 m^2/g

but decreased to an average of ~232 m²/g suggesting about 64% decline in surface area. The pore size also increased from an average of 5 nm—7 nm at the end of the 40 h, representing about 28% pore size enlargement, which consequently led to the observed decline in the total pore volume of all the catalysts. The pores enlargement denoted some deformation of the ordered mesopores that is confirmed by the narrowing and flattening of the isotherms in

^b Variation range ±2%.

supplemental Fig 12. It is interesting that despite this substantial decrease in surface area as well as the loss of ordered mesoporosity, all the other catalysts except 15%Ni-SBA-15, retained stability and >80% glycerol conversion for the entire 40 h. This observation underpins the fact that the catalyst performance and turnover frequencies are somewhat structure insensitive as reported by Rioux et al. [59], but more dependent on the active site availability, particle size and dispersion of the active sites during long term hydrothermal GSR activity.

Conclusions

We have synthesized high surface area catalysts by one-pot hydrothermal procedure with Co and Ni metals and only in one case by impregnation of SBA-15 with Co and Ni salts. The SEM-EDX results indicate that the metal particles are uniformly distributed in the catalysts prepared by one-pot procedure. The N₂ adsorption-desorption isotherms analyses indicate highly mesoporous structure even after the addition of metals. The wide angle XRD analysis showed the formation of catalytically active nickel-cobalt mixed oxide (NiCo2O4) phase in bimetallic catalysts. Bimetallic catalysts prepared by one-pot method (10%Co-5%Ni-SBA-15) and incipient wetness impregnation (10%Co-5%Ni-SBA-15-IMPG) exhibited remarkable GSR activity and stability compared to the monometallic species. At higher temperature of 650 °C and 700 °C, the onepot and impregnated catalysts showed similar activity-both attaining 100% glycerol conversion at steady state. However, at low temperature of 450 $^{\circ}$ C, although both yielded ~62% H₂ selectivity, the one-pot catalysts showed 50% glycerol conversion compared to ~70% by the impregnated catalyst. For the monometallic catalysts, cobalt-based SBA-15 catalysts exhibited better GSR activity and higher stability than nickelbased catalysts. Incorporation of MgO in Co-SBA-15 increased both glycerol conversion (up to 99%) and catalyst stability. TGA-TPO analysis of spent catalysts showed that addition of MgO to Ni-SBA-15 decreased the amount of carbon deposition on the catalysts by as much as 66%. While catalyst stability performance followed the trend 10%Co-5%Ni > 10%Co-5% MgO >10%Co-5%Ni-IMPG > 15%Co > 10%Ni-5%MgO, glycerol conversion was observed in the order: 10%Co−5%Ni-IMPG ≥ 10%Co-5%Ni > 10%Co-5%MgO > 15%Co > 15%Ni > 10%Ni-5% MgO. It is worth noting that all the catalysts studied at the optimum temperature of 650 °C showed an impressive hydrogen selectivity of \geq 70% under our experimental conditions.

Acknowledgement

The authors acknowledge the funding received from National Science Foundation (NSF) for the NSF-CREST Bioenergy Center (Grant No. HRD-124215). We are also very grateful to Dr. Schimmel (Dept. Chair of Energy and Environmental Systems) for his additional financial support. The authors would like to thank Mr. James King (Chemistry Department) for his support in the experimental work and Mr. Bryce

Holmes (School of Agriculture and Environmental Sciences) for his help with ICP analysis. The authors thank Dr. Sankar and Dr. Yarmolenko (Center for Advanced Materials and Smart Structures-CAMSS) at NCAT for the use of the XRD for material characterization. We also thank the Joint School of Nanoscience and Nanoengineering for the use of their SEM and TEM facilities.

REFERENCES

- [1] Boudghene Stambouli A, Traversa E. Fuel cells, an alternative to standard sources of energy. Renew Sustain Energy Rev 2002;6(3):295–304.
- [2] Stambouli AB, Traversa E. Solid oxide fuel cells (SOFCs): a review of an environmentally clean and efficient source of energy. Renew Sustain Energy Rev 2002;6(5):433-55.
- [3] Steele BCH, Heinzel A. Materials for fuel-cell technologies. Nature 2001;414(6861):345–52.
- [4] Song C. Global challenges and strategies for control, conversion and utilization of CO₂ for sustainable development involving energy, catalysis, adsorption and chemical processing. Catal Today 2006;115(1–4):2–32.
- [5] Pérez-Hernández R, et al. Hydrogen production by methanol steam reforming over Pd/ZrO2-TiO2 catalysts. Top Catal 2011;54(8-9):572-8.
- [6] Jiang C, et al. Kinetic study of steam reforming of methanol over copper-based catalysts. Appl Catal Gen 1993;93(2):245-55.
- [7] Hur E, Moon DJ. Steam reforming of glycerol into hydrogen over nano-size Ni-based hydrotalcite-like catalysts. J Nanosci Nanotechnol 2011;11(8):7394—8.
- [8] Acar C, Dincer I. Comparative assessment of hydrogen production methods from renewable and non-renewable sources. Int J Hydrogen Energy 2014;39(1):1–12.
- [9] Sattler C, et al. Solar hydrogen production via sulphur based thermochemical water-splitting. Sol Energy 2017;156:30–47.
- [10] Das D, Veziroğlu TN. Hydrogen production by biological processes: a survey of literature. Int J Hydrogen Energy 2001;26(1):13—28.
- [11] Ni M, et al. An overview of hydrogen production from biomass. Fuel Process Technol 2006;87(5):461–72.
- [12] Rogelj J, et al. Paris Agreement climate proposals need a boost to keep warming well below 2 degrees C. Nature 2016;534(7609):631–9.
- [13] Silva JM, Soria MA, Madeira LM. Challenges and strategies for optimization of glycerol steam reforming process. Renew Sustain Energy Rev 2015;42:1187–213.
- [14] Lin Y-C. Catalytic valorization of glycerol to hydrogen and syngas. Int J Hydrogen Energy 2013;38(6):2678–700.
- [15] San-José-Alonso D, et al. Ni, Co and bimetallic Ni—Co catalysts for the dry reforming of methane. Appl Catal Gen 2009;371(1–2):54–9.
- [16] Vaidya PD, Rodrigues AE. Glycerol reforming for hydrogen production: a review. Chem Eng Technol 2009;32(10):1463–9.
- [17] Zhang B, et al. Hydrogen production from steam reforming of ethanol and glycerol over ceria-supported metal catalysts. Int J Hydrogen Energy 2007;32(13):2367-73.
- [18] Hirai T, et al. Production of hydrogen by steam reforming of glycerin on ruthenium catalyst. Energy Fuel 2005;19(4):1761–2.
- [19] Czernik S, et al. Hydrogen by catalytic steam reforming of liquid byproducts from biomass thermoconversion processes. Ind Eng Chem Res 2002;41(17):4209-15.
- [20] Adhikari S, Fernando S, Haryanto A. Production of hydrogen by steam reforming of glycerin over alumina-supported metal catalysts. Catal Today 2007;129(3–4):355–64.

- [21] Koh AC, et al. Hydrogen or synthesis gas production via the partial oxidation of methane over supported nickel—cobalt catalysts. Int J Hydrogen Energy 2007;32(6):725—30.
- [22] Sanchez EA, Comelli RA. Hydrogen production by glycerol steam-reforming over nickel and nickel-cobalt impregnated on alumina. Int J Hydrogen Energy 2014;39(16):8650-5.
- [23] Busca G, et al. Nickel versus cobalt catalysts for hydrogen production by ethanol steam reforming: Ni-Co-Zn-Al catalysts from hydrotalcite-like precursors. Int J Hydrogen Energy 2010;35(11):5356-66.
- [24] Papageridis KN, et al. Comparative study of Ni, Co, Cu supported on γ-alumina catalysts for hydrogen production via the glycerol steam reforming reaction. Fuel Process Technol 2016;152:156–75.
- [25] Denis A, et al. Steam reforming of ethanol over Ni/support catalysts for generation of hydrogen for fuel cell applications. Catal Today 2008;137(2-4):453-9.
- [26] Muñoz M, Moreno S, Molina R. The effect of the absence of Ni, Co, and Ni–Co catalyst pretreatment on catalytic activity for hydrogen production via oxidative steam reforming of ethanol. Int J Hydrogen Energy 2014;39(19):10074–89.
- [27] Barroso-Martin I, et al. Au and AuCu nanoparticles supported on SBA-15 ordered mesoporous titania-silica as catalysts for methylene blue photodegradation. Materials 2018;11(6).
- [28] He C, Tian B, Zhang J. Synthesis of thermally stable and highly ordered bicontinuous cubic mesoporous titania—silica binary oxides with crystalline framework. Microporous Mesoporous Mater 2009;126(1–2):50–7.
- [29] Zhao M, Church TL, Harris AT. SBA-15 supported Ni-Co bimetallic catalysts for enhanced hydrogen production during cellulose decomposition. Appl Catal B Environ 2011;101(3-4):522-30.
- [30] Leofanti G, et al. Surface area and pore texture of catalysts. Catal Today 1998;41(1):207—19.
- [31] Sing KS, et al. Reporting physisorption data for gas/solid systems. Handbook of Heterogeneous Catalysis; 2008.
- [32] Abrokwah RY, Deshmane VG, Kuila D. Comparative performance of M-MCM-41 (M: Cu, Co, Ni, Pd, Zn and Sn) catalysts for steam reforming of methanol. J Mol Catal Chem 2016;425:10–20.
- [33] Wang J, et al. Characterizations of the thermal decomposition of brucite prepared by sol-gel technique for synthesis of nanocrystalline MgO. Mater Lett 1998;35(5):317–23.
- [34] Ahmadvand H, et al. Exchange bias in Co/CoO/Co3O4 nanostructures. J Magn Magn Mater 2015;377:19–23.
- [35] Chiou JY, et al. Steam reforming of ethanol over CoMg/SBA-15 catalysts. 2013.
- [36] Huang Z-D, et al. Preparation and characterization of SBA-15 supported cobalt—molybdenum sulfide catalysts for HDS reaction: an all sulfide route to hydrodesulfurization catalysts. Catal Lett 2008;124(1–2):24–33.
- [37] Calles J, et al. Hydrogen production by glycerol steam reforming over SBA-15-supported nickel catalysts: effect of alkaline earth promoters on activity and stability. Catal Today 2014;227:198–206.
- [38] Ahmadvand H, et al. Exchange bias in Co/CoO/Co3O4 nanostructures. J Magn Magn Mater 2015;377:19–23.
- [39] Brunauer S, et al. On a theory of the van der Waals adsorption of gases. J Am Chem Soc 1940;62(7):1723–32.
- [40] Luisetto I, Pepe F, Bemporad E. Preparation and characterization of nano cobalt oxide. J Nanoparticle Res 2008;10(1):59-67.
- [41] Tang C-W, Wang C-B, Chien S-H. Characterization of cobalt oxides studied by FT-IR, Raman, TPR and TG-MS. Thermochim Acta 2008;473(1-2):68-73.

- [42] Kruatim J, Jantasee S, Jongsomjit B. Improvement of cobalt dispersion on Co/SBA-15 and Co/SBA-16 catalysts by ultrasound and vacuum treatments during postimpregnation step. Eng J 2017;21(1):17–28.
- [43] Afzal M, Theocharis CR, Karim S. Temperature programmed reduction of silica supported nickel catalysts. Colloid Polym Sci 1993;271(11):1100-5.
- [44] Koh A, et al. Hydrogen or synthesis gas production via the partial oxidation of methane over supported nickel—cobalt catalysts. Int J Hydrogen Energy 2007;32(6):725—30.
- [45] Klissurski D, Uzunova E, Ivanov K. Binary spinel cobaltites of nickel, copper and zinc as precursors of catalysts for carbon oxides methanation. Catal Lett 1992;15(4):385–91.
- [46] Klissurski D, Uzunova E. Synthesis of nickel cobaltite spinel from coprecipitated nickel-cobalt hydroxide carbonate. Chem Mater 1991;3(6):1060-3.
- [47] Vizcaíno AJ, Carrero A, Calles JA. Hydrogen production by ethanol steam reforming over Cu—Ni supported catalysts. Int J Hydrogen Energy 2007;32(10—11):1450—61.
- [48] Vizcaíno A, Carrero A, Calles J. Ethanol steam reforming on Mg-and Ca-modified Cu–Ni/SBA-15 catalysts. Catal Today 2009;146(1):63–70.
- [49] Zamzuri NH, et al. Hydrogen production from catalytic steam reforming of glycerol over various supported nickel catalysts. Int J Hydrogen Energy 2017;42(14):9087–98.
- [50] Huang Z-D, et al. Preparation and characterization of SBA-15 supported cobalt—molybdenum sulfide catalysts for HDS reaction: an all sulfide route to hydrodesulfurization catalysts. Catal Lett 2008;124(1):24.
- [51] Li G, et al. One-pot pyrolytic synthesis of mesoporous MCo2O4(4.5) (M=Mn, Ni, Fe, Cu) spinels and its high efficient catalytic properties for CO oxidation at low temperature. J Mol Catal Chem 2014;390:97–104.
- [52] Chen J. Hydrogen production by the steam reforming of bioethanol over nickel-based catalysts for fuel cell applications. Int J Sustain Green Energy 2017;6(3):28.
- [53] Li S, Gong J. Strategies for improving the performance and stability of Ni-based catalysts for reforming reactions. Chem Soc Rev 2014;43(21):7245–56.
- [54] Calles JA, et al. Hydrogen production by glycerol steam reforming over SBA-15-supported nickel catalysts: effect of alkaline earth promoters on activity and stability. Catal Today 2014;227:198–206.
- [55] Atchudan R, et al. Synthesis and characterization of graphitic mesoporous carbon using metal-metal oxide by chemical vapor deposition method. Microporous Mesoporous Mater 2015;215(1387–1811):123–32.
- [56] Carreon MA, et al. Mesoporous nanocrystalline mixed metal oxides from heterometallic alkoxide precursors: cobalt—nickel oxide spinels for propane oxidation. Eur J Inorg Chem 2006;2006(24):4983—8.
- [57] Choong CK, et al. Effect of calcium addition on catalytic ethanol steam reforming of Ni/Al 2 O 3: I. Catalytic stability, electronic properties and coking mechanism. Appl Catal Gen 2011;407(1):145-54.
- [58] Esparza J, et al. N 2 sorption scanning behavior of SBA-15 porous substrates. Colloid Surface Physicochem Eng Aspect 2004;241(1):35–45.
- [59] Rioux RM, et al. High-surface-area catalyst Design: synthesis, characterization, and reaction studies of platinum nanoparticles in mesoporous SBA-15 silica. J Phys Chem B 2005;109(6):2192–202.